08

The method of crystalline nanostructures formation from amorphous vanadium dioxide films

© A.I. Komonov,[1] N.D. Mantsurov,[1] B.V. Voloshin,[1] V.A. Seleznev,[1] V.N. Kichay,[2] L.V. Yakovkina,[2] S.V. Mutilin[1]

[1] Rzhanov Institute of Semiconductor Physics, Siberian Branch, Russian Academy of Sciences, 630090 Novosibirsk, Russia
[2] Nikolaev Institute of Inorganic Chemistry, Siberian Branch, Russian Academy of Sciences, 630090 Novosibirsk, Russia
e-mail: komonov@isp.nsc.ru

Received April 23, 2025
Revised April 23, 2025
Accepted April 23, 2025

This work proposes a precise technique for the vanadium dioxide crystalline nanostructures formation from thin solid amorphous vanadium oxide films grown on silicon substrates. High accuracy of the formed nanoscale structures is achieved via using atomic layer deposition and oxidation scanning probe lithography methods. The amorphous nanostructures undergo crystallization following temperature annealing in vacuum. The size of the formed nanocrystals is defined by the thickness of the initial amorphous film and the geometry of the amorphous nanostructures. In this work we obtained single polycrystalline nanostructures and ordered arrays of nanostructures. Lateral dimensions of crystalline nanostructures are less than 100 nm. The single vanadium dioxide nanocrystals are less than 5 nm in height and less than 50 nm in diameter.

Keywords: Atomic layer deposition, oxidation scanning probe lithography, post-growth annealing, vanadium dioxide nanostructures, vanadium dioxide nanocrystals.

DOI: 10.61011/TP.2025.09.61848.73-25

Introduction

Due to a number of advantages, the oxide electronics is more and more applied in various fields of science and technology and supplements the classic silicon electronics with its functional [1]. One of the most promising trends in the oxide electronics is vanadium oxides that have an extensive nomenclature, whose application field is constantly expanded [2]. Among all the vanadium oxides, the most attractive is vanadium dioxide (VO_2) due to the fact that it has a reversible semiconductor-metal phase transition at 340 K [3]. At the same time, crystalline and electron structures of VO_2 undergo significant changes that are accompanied with variation of conductivity by up to 5 orders [4] and variation of optical properties ($\Delta n \sim 1$ when $\lambda \sim 1500$ nm) [5]. An important specific feature of VO_2 for practical applications is that in addition to the temperature the phase transition can be also initiated by the electric field [6], the magnetic field [7], laser radiation [8], mechanical stresses [9], etc. Besides, doping of VO_2 makes it possible to shift the temperature of the phase transition and to significantly affect other properties of VO_2 [10]. Therefore, the field of application of VO_2 is very wide and includes sensors and micro-actuators [11], thermochromic smart coatings [12], photovoltaic keys [13], tunable metastructures [14], neuromorphic systems [15] and many others [16]. The most modern instruments based on VO_2 are created on thin films, which have an essential problem of mechanical strength of the formed structures due to mechanical stresses that are caused by a structural transition of the crystalline lattice from a monoclinic into a tetragonal one [17]. Actually, with the phase transition, the lattice constant varies approximately by 1 % [18]. A cyclic switching results in degradation of the VO_2 crystalline films and instrument structures based thereon withstand at most 10^8 switching cycles [19]. It is known that in nanoscale structures stresses that occur during the phase transition do not reach critical values which cause irreversible degradation [20]. Therefore, actively underway are the search of new methods of formation of the VO_2 nanostructures and developments of a technology of manufacturing instrument devices based thereon [21]. There are two approaches to forming the nanostructures — „from top to bottom“ and „from bottom to top“ [22]. The first one means forming separate nanostructures and their arrays from solid films, including selective etching of the thin films. The second approach is synthesis of the nanostructures from separate atoms and molecules. Many methods of synthesis of the VO_2 nanocrystals are known — it is a sol-gel method [23], a hydrothermal method [24], pulsed laser deposition [25], chemical vapor deposition [26], etc. We have proposed a method of selective synthesis of arrays of single-crystal nanocrystal and nanowires by chemical vapor deposition on pre-nanostructured silicon substrates [27,28]. As a result, the VO_2 nanocrystals selectively grew up in pre-defined locations. Electrical measurements of these structures have shown that it was possible to form single crystals of quite small sizes, in which energy spent for the phase transition

did not exceed 4.2 fJ, while the number of switchings exceeds $2 \cdot 10^{11}$ with complete preservation of the crystal characteristics. Thus, high response time and low energy consumption is attained in such small structures, wherein the phase transition has only elastic strain. However, the technology of synthesis „from bottom to top“ is not always applicable and the formed structures are not planar. The main method of formation of the VO_2 3*D*-nanostructures from the thin solid films is lithography [29]. Application of the methods of optical and electron-beam lithography for nanostructuring of crystalline and polycrystalline VO_2 films often results in formation of the nanostructures with unreproducible characteristics. Actually, it is difficult to completely remove organic resists applied in the lithography and, consequently, it results in substantial degradation of characteristics of the produced structures [30,31]. There is a known method of non-resist nanostructuring of the thin polycrystalline VO_2 films using scanning probe lithography [32]. Unfortunately, it is hard to use this method to form nanostructures with sizes less than the VO_2 nanocrystals that make up the initial thin polycrystalline VO_2 film. Additionally, the polycrystalline structure, namely, the presence of interfaces between film grains prevents precise positioning of the formed elements and limits a density of the array elements. Previously, we were the first to propose a method of forming amorphous VO_2 nanostructures from solid amorphous vanadium oxide films by oxidation scanning probe lithography (OSPL) [33]. This method is actively applied for lithography of various metal and semiconductor thin films as well as two-dimensional materials [34]. We have shown in the study [35] that annealing of solid amorphous vanadium oxide films results in formation of unordered arrays of the VO_2 nanocrystals. We have systematically studied and described in detail optimal conditions of post-growth annealing for reproducible synthesis of the VO_2 nanocrystals of the M1 phase. It also included investigation of the influence of a composition of the initial amorphous film on a quality of the formed nanocrystals. Electrical measurements of these structures have shown that the formed arrays of the VO_2 nanocrystals have high stability (more than 10^{10} switching cycles) and the switching energy is less than 150 fJ, which is significantly lower than in the film structures.

Within the framework of development of a methodology for forming the vanadium oxide nanostructures using OSPL, we have published a cycle of papers that describe in detail the influence of the main factors on the probe oxidation process. Thus, the study [36] has established a fact of oxidation of amorphous unsaturated-vanadium-oxide films using scanning probe lithography, identified the influence of the composition of the oxidized film on the nanostructuring process and determined a threshold voltage, at which stable film oxidation processes occur. It was found in the study [33] that the probe oxidation process is OSPL that results in formation of less dense saturated vanadium pentoxide (V_2O_5), which, as shown, is fully soluble in water. It also studied the influence of the main OSPL parameters such as a value and duration of the applied voltage, relative humidity of the environment, a thickness of the oxidized film. It is found that the time dependence of the thickness of the oxidized nanostructures is of a logarithmic nature and is well approximated by the Cabrer-Mott model. A model of the occurring processes is proposed. The array of nanowells of the diameter of about 10 nm and the depth of 0.3 nm is produced. The study [37] was the first to carry out OSPL of the polycrystalline VO_2 films that had been produced by chemical vapor deposition. It is found that the oxidation process occurs only at the air's relative humidity of 50 %. The main factors affecting the process of OSPL of the polycrystalline films were studied. It is shown that a process of local anode oxidation is described with good accuracy by the Carber-Mott model. The amorphous V_2O_5 being formed increases a local volume of the film approximately in two times and fully dissolves in water. The study [38] was the first to form an array of the amorphous VO_2 nanoislands by means of raster OSPL with a defined geometry and a defined density of elements from a solid amorphous VO_2 film. The study [39] was the first to form hierarchic arrays of the VO_2 nanostructures by means of raster OSPL from a solid amorphous VO_2 film. It is found that a thin V_2O_5 layer is constantly formed on the surface of the amorphous VO_2 film in the normal conditions of the environment. It is shown that by cyclic removal of the formed intrinsic V_2O_5 oxide in water it is possible to controllably reduce sizes of the array elements as well as to remove a residual layer of the VO_2 film to the silicon substrate, thereby forming arrays of free-standing VO_2 nanoislands. The obtained practices for OSPL of the vanadium oxide films allow us to create precise amorphous VO_2 nanostructures.

The aim of the present study is to design a method of forming the crystalline VO_2 nanostructures by successive nanostructuring of the amorphous VO_2 films by means of OSPL and subsequent annealing of the produced amorphous nanostructures. At the same time, it is expected that using the amorphous VO_2 nanostructures with accurately defined sizes and in accurately defined areas of the sample will allow controllably creating during annealing precise crystalline VO_2 nanostructures that are applicable for creating instruments for nanoelectronics and nanophotonics.

1. Experimental procedure

The thin VO_2 films were synthesized by plasma-enhanced (PE) atomic layer deposition (ALD) in the installation SI ALD LL (Sentech, Germany) [40,41]. The power of a capacitively couples plasma source is 200 W, while its frequency is 13.56 MHz. The reactor was equipped with a laser ellipsometer for monitoring the ALD process in real time (ALD-RTM, Sentech) [42]. All the films have been grown on the silicon substrates (100) of the *n*-type with resistivity of 0.005 Ω·cm. Before being loaded into the reactor, the substrates were chemically processed in the mixture $H_2SO_4 : H_2O_2 = 3 : 1$ for 15 min and then flushed in distilled water and dried in a jet of clean dry air. The films

were synthesized by the ALD method in the reactor under the pressure of 30 Pa and at the temperature of 150 °C. Tetrakisethylmethylaminovanadium (TEMAV) was used as a vanadium precursor, whose decomposition temperature Tdecomp is about 175 °C [43,44]. Argon (Ar) of high purity (99.9998 %) was used as a TEMAV gas carrier, for blowing the reactor chamber and for plasma generation as well. A mixture of oxygen (O_2) 1 % and Ar was used for decomposition of the precursor into VO_2 and volatile compounds. Dynamics of the deposition process and the thickness of the vanadium oxide films were recorded *in situ* by the ellipsometry method. The ellipsometric measurements were carried out on a surface of the silicon substrate at the wavelength of 632.8 nm. The thickness of the films was obtained from the measured ellipsometric data of the parameters Ψ and Δ in a single-layer with a fixed refractive index of 2.2.

The composition of the amorphous films was determined by X-ray photoelectron spectroscopy (XPS) in the installation ProvenX-ARPES (SPECS, Germany), which is equipped with the electron energy analyzer ASTRAIOS 190 and the 2D-CMOS electron detector. An excitation source was focused monochromatic radiation Al Kα ($h\nu = 1486.7$ eV, the width of an X-ray beam at half maximum was 0.5 mm at the anode power of 150 W). The XPS spectra were recorded under normal radiation and at constant transmission energy of 30 eV with absolute energy resolution ≤ 0.6 eV. The spectrometer energy scale was calibrated by a binding energy of the Ag$3d_{5/2}$ line, which was (368.22 ± 0.05) eV in relation to the Fermi level. The XPS spectra were analyzed according to the paper [45] using the SpecsLab Prodigy software. A Shirley function was used to subtract the background. The XPS signals of O1s and V2p were fitted to mixed Lorentz-Gauss curves with a 33 % Lorentz nature.

To carry out OSPL and to subsequently study the obtained results, the atomic-force microscope NTEGRA AURA (NT-MDT, Russia) was used. The conducting AFM probes coated by tungsten carbide HA_C/W2C (Tipsnano, Estonia) and equipped with a tip of the curvature radius of below 35 nm were used. All the conducting probes were checked for presence of high conductivity by means of a special calibration sample (a silicon plate coated with the gold film). In order to form the defined-geometry nanostructures, respective templates for raster OSPLE were created. They are raster black-and-white images, in which the black color characterizes portions to be oxidized, while the white color characterizes portions which are not oxidized. The raster OSPL of all the portions of the amorphous VO_2 film was carried out at the speed of 2 μm/s with the bias voltage of 8 V and a step between the oxidized points 10 nm. In all the experiments, the positive potential was applied to the sample, while the AFM probe was grounded. After OSPL, lateral sizes of the formed nanostructures were correctly measured by using the silicon probes HA_FM (Tipsnano, Estonia) with a tip curvature radius of below 10 nm. The OSPL experiments were carried out with constantly maintaining the temperature of the environment within the range from 22 °C to 24 °C and the air's relative humidity within the range from 20 % to 30 %. The obtained data of the AFM images were analyzed using the Gwyddion open-source software for analysis and processing the SPM images. [46].

The films produced by PE ALD were annealed at the temperature of 650 °C for 2 h in a horizontal quartz reactor with hot walls (resistive heater). The partial pressure of oxygen in the reactor was 1.4 Pa. The rate of heating and cooling down the samples was 5 °C/min.

Presence of a crystal phase in the synthesized films was determined by means of Raman scattering (RS) at the room temperature in the back-scattering geometry in the spectrometer T64000 (Horiba Jobin Yvon, Japan) with spectral resolution of 0.5 cm^{-1}. A optic fiber laser with the wavelength of 514.5 nm was used for excitation. The Raman scattering spectra were recorded in a micro-Raman scattering mode using the optical microscope BX41 (Olympus, Japan) with a lens of magnification $\times 100$. In order to avoid local heating of the films with a diagnostic laser beam, the sample was placed just below a focal plane. The laser beam power on the sample surface did not exceed 1 mW with the spot diameter of 5 μm.

2. Results and discussion thereof

In order to form the crystalline nanostructures from the amorphous vanadium dioxide film, we used PE ALD to produce a series of structures, which was characterized by the thickness of the VO_2 films from 3 to 16 nm. The thickness of the used films was defined by duration of the synthesis process. The elementary composition of the produced films was determined by the XPS method. A position of and a form of the lines of the V$2p_{3/2}$ peak were taken to determine a state of vanadium. In the provided spectrum (Fig. 1), this peak corresponds to the vanadium

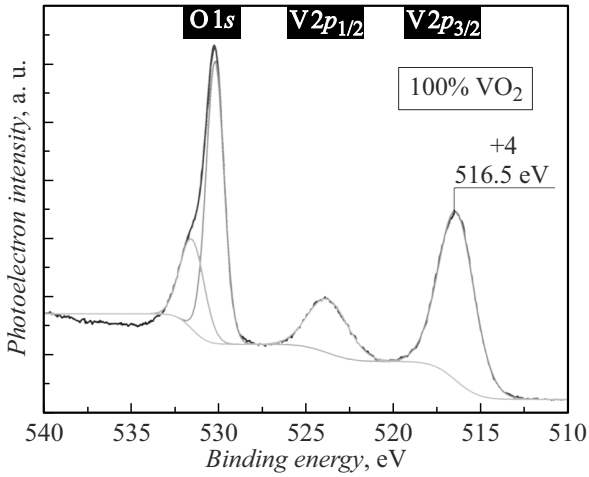

Figure 1. XPS spectrum of the VO_2 film. The V $2p_{3/2}$ corresponds to the vanadium oxidation degree +4.

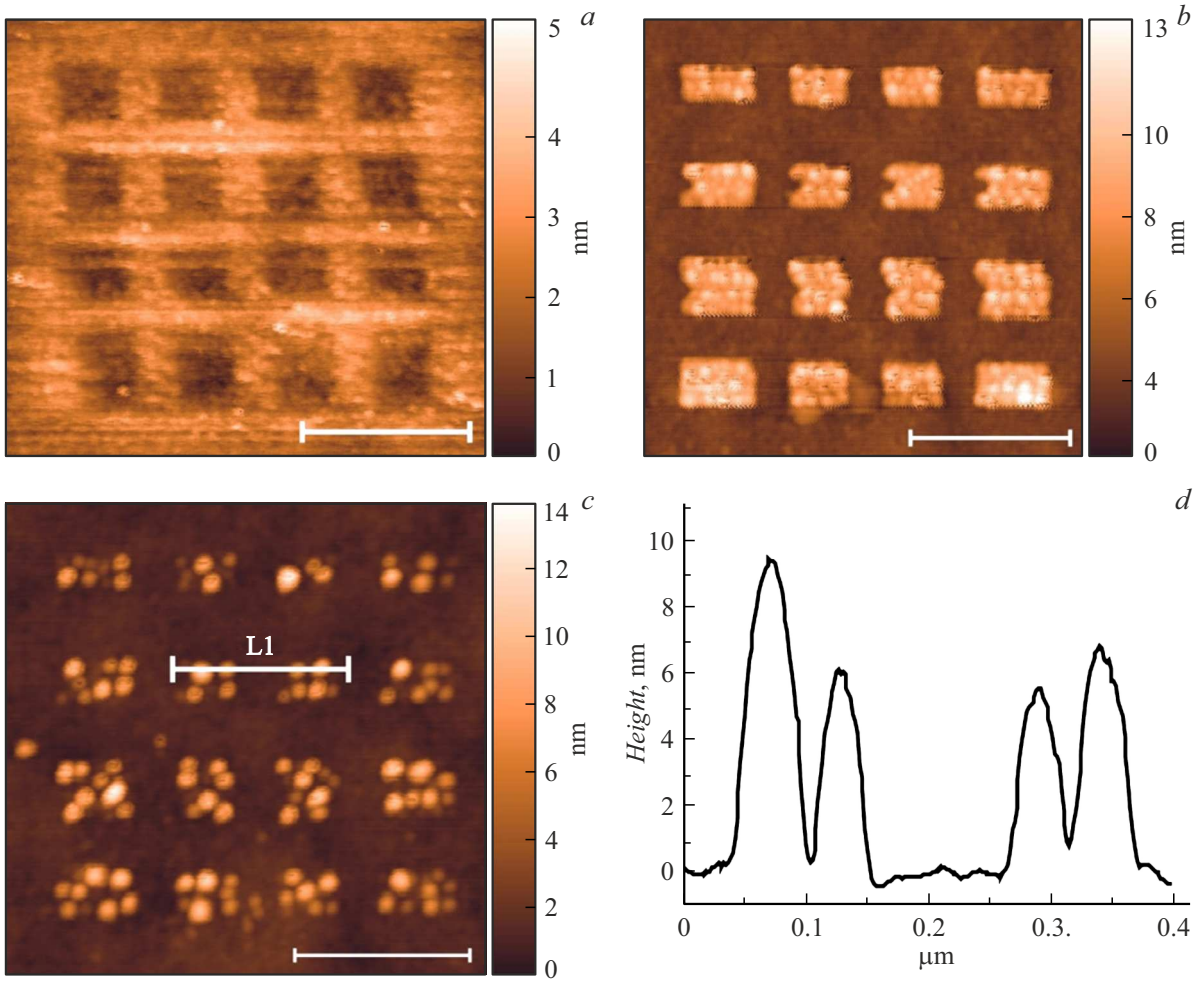

Figure 2. AFM images of the stages of formation of the VO_2 nanostructures: *a* — oxidation of the whole surface except for the 4×4 array of the nanostructures; *b* — removal of the formed V_2O_5; *c* — formation of the VO_2 nanocrystals after annealing; *d* — the profile along the line L1 in Fig. 2, *c*. The length of a dimensional section is 400 nm.

oxidation degree +4. Whence, it can be concluded that the film completely consists of vanadium oxide (IV).

The previous oxidation experiments have shown that when carrying out single-type oxidation procedures during OSPL of the thin amorphous VO_2 films the sizes of the formed structures can differ from each other by 30 – 70 % [33]. Consequently, in order to increase reliability of the study, the arrays of the nanostructures were formed in the form of amorphous islands. Fig. 2, *a* shows the AFM image of the 4×4 array that consists of square islands of the initial VO_2 film of the size 200×200 nm each. An area outside the islands was oxidized to saturated water-soluble V_2O_5 by means of raster OSPL under effect of voltage of 8 V. After treatment of the sample in deionized water for several seconds a part of the oxidized film was removed to the substrate. It resulted in formation of the array of separate rectangular nanoislands of the amorphous VO_2 film (Fig. 2, *b*). At the same time, we relate the change of the form of the nanoislands to specific features of operation of the AFM software during probe lithography, during which the part of the film was removed within lithographic squares, which were not to be oxidized. It resulted in formation of the rectangular regions. After annealing, the amorphous VO_2 nanoislands were replaced by groups of the VO_2 nanocrystals (Fig. 2, *c*). It is clear from the profile L1 in Fig. 2, *c* that each nanostructured region is a group of the nanocrystals of the height of at least 5 nm and the diameter of at least 50 nm.

The VO_2 crystal phase M1 is confirmed by the RS method. Fig. 3 shows the RS spectrum of the sample with the nanocrystals. The most intense peak with the maximum at 520.5 cm^{-1} is related to scattering at optical long-wavelength phonons of the first order in the silicon substrate. Vertical dashed lines mark 14 Raman modes of the monoclinic (M1) semiconductor phase of VO_2. The (M1) monoclinic phase of VO_2 of the spatial group P21/c has 18 Raman active modes with the symmetries Ag and Bg [47]. The majority of these modes is visible at the room temperature in our samples. The most low-frequency peak, which is near 142 cm^{-1} is ascribed to soft phonon

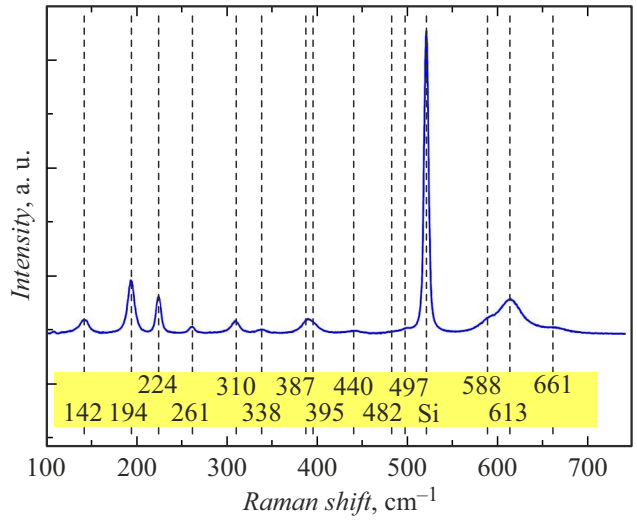

Figure 3. RS spectrum of the sample with the crystalline VO_2 nanostructures.

oscillations. The peaks at 194, 224 cm^{-1} are related to motion of the V-V bonds. The other peaks at 261, 310, 338, 387, 395, 440, 482, 497, 588, 613, 661 cm^{-1} are related to vibrational modes of the V-O bonds [47,48].

Fig. 4 shows a diagram of the process of formation of the crystalline VO_2 nanostructures. It is known that when voltage is applied between a needle of the AFM probe and the vanadium oxide surface, the electric field reaches its maximum values directly near the needle surface and quickly decreases with distance from the probe [49]. In conditions of the normal humidity, a thin water film is always on the surface of the structures, therefore, a water layer is arranged between the needle and the surface of the VO_2 film. Under effect of the electric field the water molecules dissociate to anions and cations. The strong electric field result in local flow of ion currents in the area between the needle tip and the sample surface. The electric field also contributes to migration of the anions to the sample surface, where in our case they react with the vanadium atoms on the surface of the VO_2 film The ion flux between the tip of the AFM probe and the sample forms the Faraday current. Oxidation-reduction reactions which occur at the same time are described by the following equations:

the complete equation:

$$2VO_2 + H_2O \rightarrow V_2O_5 + H_2 \uparrow, \quad (1)$$

the cathode (needle):

$$2H^+ + 2e \rightarrow H_2 \uparrow, \quad (2)$$

the anode (sample):

$$2VO_2 + 2OH^- - 2e \rightarrow V_2O_5 + H_2O. \quad (3)$$

When applying the voltage between the AFM probe and the conducting substrate, there is a current that oxidizes the amorphous VO_2 to V_2O_5 in an area near the needle tip (Fig. 4, *a*). With short-term (5–10 s) immersion of the structure into deionized water, the oxidized regions dissolve and only the portions of the initial amorphous VO_2 film remain (Fig. 4, *b*, *c*). After this, during annealing, the amorphous VO_2 nanostructures are transformed into the VO_2 nanocrystals (Fig. 4, *d*). Thus, it is possible to form separate nanocrystals as well as the array of the VO_2 nanocrystals.

If the film is only partially oxidized (not along its entire thickness) as shown in Fig. 5, then as a result of dissolution in water and subsequent annealing the VO_2 nanocrystals are formed on the entire surface of the substrate. At the same time, in locations where the film is thinner, the finer VO_2 crystals are formed. Fig. 5, *a*, *d* shows an initial central portion of the VO_2 film, which is preserved as a result of treatment in water (Fig. 5, *b*, *e*). During annealing, the central part (where the VO_2 film of the initial thickness is preserved) has the larger VO_2 nanocrystals formed (Fig. 5, *c*, *f*). Thus, it is possible to combine formation of the separate nanocrystals on the surface of the Si substrate and formation of the nanocrystals of the various size by varying the thickness of the film to be annealed. At the same time, it is important to note that the sizes of the nanocrystals formed as a result of annealing increase with increase of the thickness of the initial film.

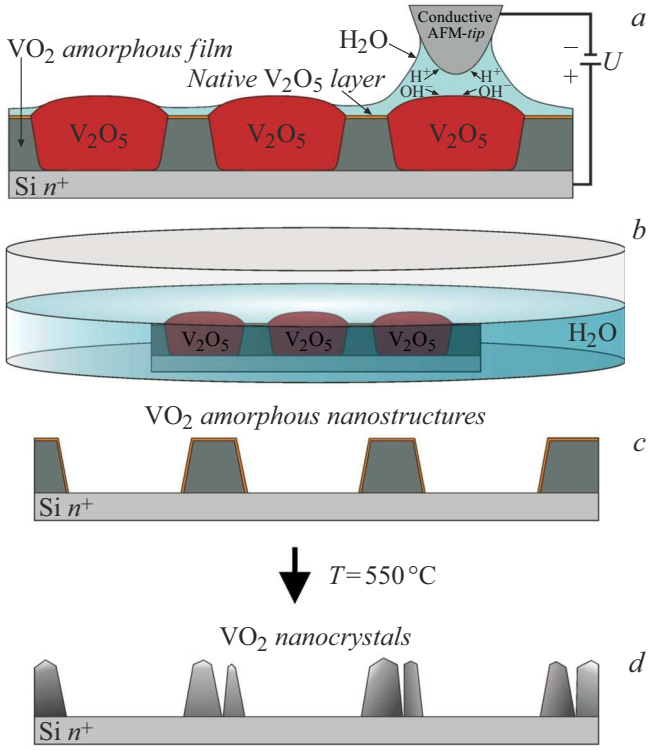

Figure 4. Schematic image of formation of the crystalline VO_2 nanostructures: *a* — local oxidation of the amorphous VO_2 film to V_2O_5; *b* — selective removal of V_2O_5 in water; *c* — the formed amorphous VO_2 nanostructures; *d* — the crystalline VO_2 nanostructures formed as a result of annealing.

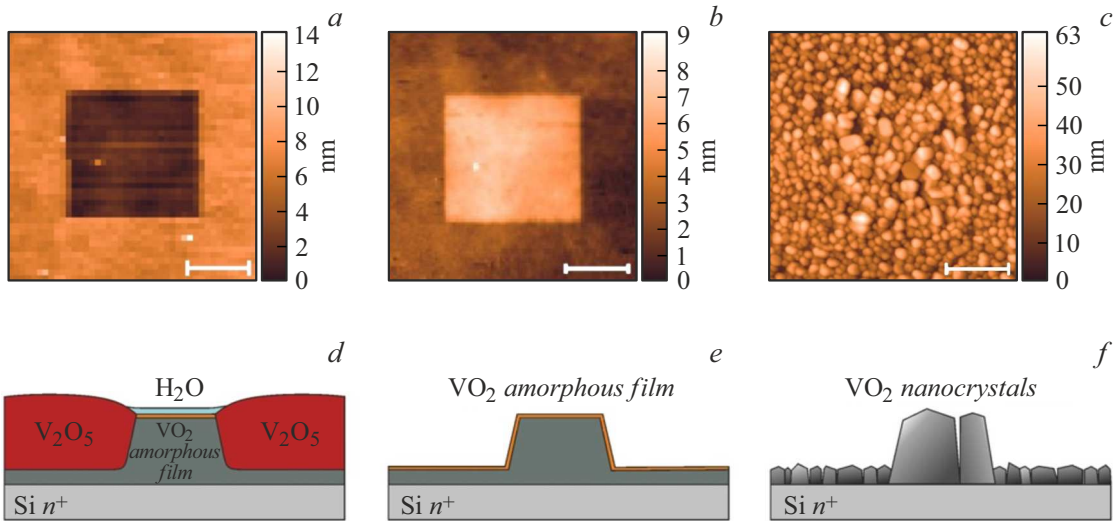

Figure 5. AFM images and the schematic images of the stages of formation of the VO_2 nanocrystals of the various sizes: *a* — formation of the square VO_2 nanostructure by the OSPL method; *b* — selective removal of the formed V_2O_5 layer in water; *c* — formation of the crystalline VO_2 nanostructures of the various sizes as a result of annealing; *d* — the schematic image of *a*; *e* — the schematic image of *b*; *f* — the schematic image of *c*. The length of a dimensional section is 500 nm.

We note an important point that is typical for the vanadium oxide structures. In the normal conditions, in air, the surface of the unsaturated vanadium oxides has a thin natural V_2O_5 oxide formed, and it has a thickness that usually does not exceed 2–3 nm. At the same time, the saturated oxide is stable despite the fact that the sample surface is coated with the thinnest water nanofilm. Actually, it is known that a rate of the reaction of dissolution of V_2O_5 in water largely depends on pH. The higher pH, the slower the process of dissolution. But interaction of V_2O_5 with water results in formation of acid HVO_3, which increases acidity of the water nanofilm, thereby multiply decelerating the rate of the occurring reaction [50], which is a limiting factor of dissolution of the natural V_2O_5 oxide on the surface of the VO_2 nanostructures in the natural conditions.

Now we consider with more details the influence of the thickness of the initial VO_2 film on the size of the formed VO_2 nanocrystal after annealing. Fig. 6 shows dependences of a height and a volume of the formed VO_2 nanocrystals on the thickness of the initial amorphous VO_2 film. Increase of the film thickness results in increase of the sizes of the VO_2 nanocrystals.

The presented method allows controllably forming complex micro- and nano-structures that consist both of the single VO_2 nanocrystals as well as the ordered arrays of the polycrystalline portions of the structures. Fig. 7, *a* exemplifies the complex VO_2 nanostructures that are formed by means of the OSPL on the surface of the amorphous VO_2 films. After treatment in water, the portion of the amorphous VO_2 film, which was fully oxidized, is removed and only the nanostructures (non-oxidized portions of the film) are preserved (Fig. 7, *b*). It is clear in Fig. 7, *c* that during annealing the produced amorphous

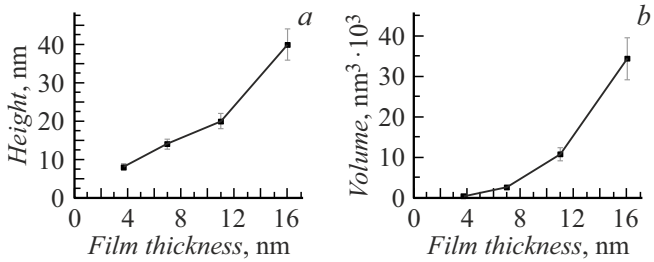

Figure 6. Dependences of the height (*a*) and the volume (*b*) of the single VO_2 nanocrystals in the formed VO_2 nanostructures on the thickness of the modified amorphous VO_2 film.

nanostructures the nanocrystals are formed only in an area, which was previously occupied by the amorphous nanostructures. Below and above in the center of Fig. 7, *c*, there are visibly two rings of the VO_2 nanocrystals with the internal and external diameters of 550 and 650 nm for the small rings and 600 and 950 nm for the large ring, respectively. On the left in the center of Fig. 7, *c*, there is visibly a rhomb of the VO_2 nanocrystals with a side of 600 nm as well as a separate group of the nanocrystals in the center. On the right above in Fig. 7, *c*, there is visibly a C-shaped ring of the VO_2 nanocrystals with the internal and external diameters of 700 and 1050 nm. At the same time, the diameters of the separate VO_2 nanocrystals in these nanostructures vary from 50 to 100 nm, while their height varies from 5 to 15 nm. Thus, it is shown that by means of OSPL of the amorphous vanadium oxide films and subsequent temperature annealing, there is formation of both the single polycrystalline nanostructures as well as the ordered arrays of the nanostructures that consist

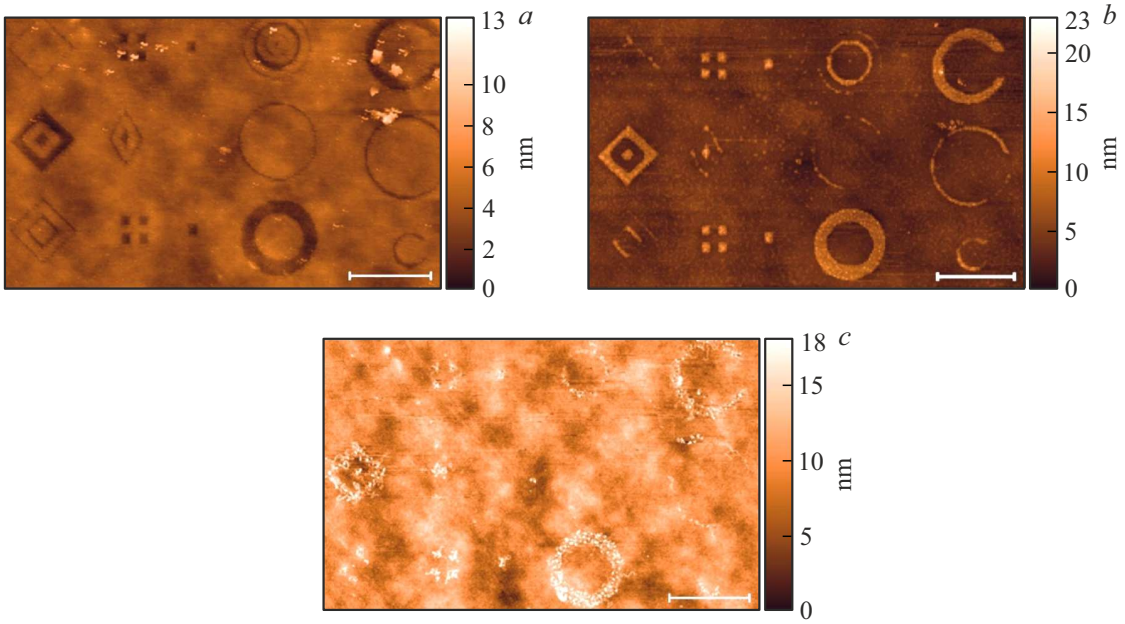

Figure 7. AFM images of the stages of formation of the various VO_2 nanostructures as rhombs, squares, rings, etc.: *a* — the image of the surface after the OSPL procedure; *b* — the image of the surface after removal of the oxidized V_2O_5 layer; *c* — the image of the surface after annealing and forming the crystalline VO_2 nanostructures. The length of a dimensional section is 1 μm.

of groups of the single nanocrystals. The array density and the geometry of the separate elements are defined by lithography. The lateral sizes of the nanostructures can be less than 50 nm, while the height thereof can be less than 10 nm. The proposed methodology allows forming the nanocrystals from the VO_2 crystals, which are promising for the elements of nanophotonics and nanoelectronics, in particular, as tunable resonators and photon crystals.

Conclusion

The study describes the methodology of forming the crystalline VO_2 nanostructures by nanostructuring of the amorphous VO_2 films by means of OSPL and subsequent annealing of the produced amorphous nanostructures. It is shown by the RS method that the formed crystalline structures have the M1 phase of VO_2. It is found that the sizes of the nanocrystals formed as a result of annealing increase with increase of the thickness of the initial film. It is shown that the developed methodology allows forming both separate polycrystalline nanocrystals with the lateral sizes of below 100 nm and above as well as the ordered arrays of the nanostructures that consists of groups of the single nanocrystals. It is also found that the size of the formed single VO_2 nanocrystals is at least 5 nm in height and at least 50 nm in diameter when annealing the initial amorphous films of the thickness of 3 nm. The presented method allows forming the micro- and nano-structures of a complex geometry as well as the single VO_2 nanocrystals, which are promising for future nanophotonics and nanoelectronics.

Acknowledgments

The RS spectra were recorded using equipment from Common Use Center „High Technologies and Nanostructured Materials“ of the Analytical-Technological Science-Research Center of the Novosibirsk State University. The XPS spectra were obtained using equipment from Common Use Center „Nanostructures“ of Rzhanov Institute of Semiconductor Physics, SB RAS. The authors would like to thank Cand. Phys.-Math. Sci. V.A. Golyashov for the obtained XPS spectra and Dr. Phys.-Math. Sci. V.A. Volodin for his help in recording the RS spectra.

Funding

This study was supported financially by the Ministry of Science and Higher Education of the Russian Federation.

Conflict of interest

The authors declare that they have no conflict of interest.

References

[1] M. Coll, J. Fontcuberta, M. Althammer, M. Bibes, H. Boschker, A. Calleja, G. Cheng, M. Cuoco, R. Dittmann, B. Dkhil, I.El Baggari, M. Fanciulli, I. Fina, E. Fortunato, C. Frontera, S. Fujita, V. Garcia, S.T.B. Goennenwein, C.-G. Granqvist, J. Grollier, R. Gross, A. Hagfeldt, G. Herranz, K. Hono, E. Houwman, M. Huijben, A. Kalaboukhov, D.J. Keeble, G. Koster, L.F. Kourkoutis, J. Levy, M. Lira-Cantu, J.L. MacManus-Driscoll, J. Mannhart, R. Martins,

S. Menzel, T. Mikolajick, M. Napari, M.D. Nguyen, G. Niklasson, C. Paillard, S. Panigrahi, G. Rijnders, F. Sánchez, P. Sanchis, S. Sanna, D.G. Schlom, U. Schroeder, K.M. Shen, A. Siemon, M. Spreitzer, H. Sukegawa, R. Tamayo, J. van den Brink, N. Pryds, F.M. Granozio. Appl. Surf. Sci., **482**, 1 (2019). DOI: 10.1016/j.apsusc.2019.03.312

[2] P. Hu, P. Hu, T. Vu, M. Li, S. Wang, Y. Ke, X. Zeng, L. Mai, Y. Long. Chem. Rev., **123**, 4353 (2023). DOI: 10.1021/acs.chemrev.2c00546

[3] A. Kumar, A. Kumar, A. Kandasami, V. Singh. J. Supercond. Nov. Magn., **37**, 475 (2024). DOI: 10.1007/s10948-024-06705-w

[4] B. Mun, K. Chen, J. Yoon, C. Dejoie, N. Tamura, M. Kunz, Z. Liu, M.E. Grass, S. Mo, C. Park, Y.Y. Lee, H. Ju. Phys. Rev. B, **84**, 113109 (2011). DOI: 10.1103/PhysRevB.84.113109

[5] A. Gonçalves, J. Resende, A.C. Marques, J.V. Pinto, D. Nunes, A. Marie, R. Goncalves, L. Pereira, R. Martins, E. Fortunato. Sol. Energy Master Sol. Cells, **150**, 1 (2016). DOI: 10.1016/j.solmat.2016.02.001

[6] G. Stefanovich, A. Pergament, D. Stefanovich. J. Phys.: Condens. Matter, **12**, 8837 (2000). DOI: 10.1088/0953-8984/12/41/310

[7] C. Wu, X. Zhang, J. Dai, J. Yang, Z. Wu, S. Wei, Y. Xie. J. Mater. Chem., **21**, 4509 (2011). DOI: 10.1039/C0JM03078C

[8] A. Cavalleri, C. Tóth, C.W. Siders, J.A. Squier, F. Raksi, P. Forget, J.C. Kieffer. Phys. Rev. Lett., **87**, 237401 (2001). DOI: 10.1103/PhysRevLett.87.237401

[9] J. Cao, E. Ertekin, V. Srinivasan, W. Fan, S. Huang, H. Zheng, J.W.L. Yim, D.R. Khanal, D.F. Ogletree, J.C. Grossman, J. Wu. Nat. Nanotechnol., **4**, 732 (2009). DOI: 10.1038/nnano.2009.266

[10] C.L. Tien, C.Y. Chiang, C.C. Wang, S.C. Lin. Materials, **17**, 2382 (2024). DOI: 10.3390/ma17102382

[11] M. Darwish, Y. Zhabura, L. Pohl. Nanomaterials, **14**, 582 (2024). DOI: 10.3390/nano14070582

[12] F. Xu, X. Cao, H. Luo, P. Jin. J. Mater. Chem. C, **6**, 1903 (2018). DOI: 10.1039/c7tc05768g

[13] C.E. Reese, A.V. Mikhonin, M. Kamenjicki, A. Tikhonov, S.A. Asher. J. Am. Chem. Soc., **126**, 1493 (2004). DOI: 10.1021/ja037118a

[14] M. Liu, R. Wei, J. Taplin, W. Zhang. Materials, **16**, 7106 (2023). DOI: 10.3390/ma16227106

[15] R. Yuan, P.J. Tiw, L. Cai, Z. Yang, C. Liu, T. Zhang, C. Ge, Ru. Huang, Y. Yang. Nat. Commun., **14**, 3695 (2023). DOI: 10.1038/s41467-023-39430-4

[16] C. Wen, L. Feng, Z. Li, J. Bai, S. Wang, X. Gao, J. Wang, W. Yao. Front. Mater., **11**, 1341518 (2024). DOI: 10.3389/fmats.2024.1341518

[17] S.A. Corr, D.P. Shoemaker, B.C. Melot, R. Seshadri. Phys. Rev. Lett., **105**, 056404 (2010). DOI: 10.1103/PhysRevLett.105.056404

[18] H. Guo, K. Chen, Y. Oh, K. Wang, C. Dejoie, S.A. Syed Asif, O.L. Warren, Z.W. Shan, J. Wu, A.M. Minor. Nano Lett., **11**, 3207 (2011). DOI: 10.1021/nl201460v

[19] A. Crunteanu, J. Givernaud, J. Leroy, D. Mardivirin, C. Champeaux, J.C. Orlianges, A. Catherinot, P. Blondy. Sci. Technol. Adv. Mater., **11**, 065002 (2010). DOI: 10.1088/1468-6996/11/6/065002

[20] F. Glas. Phys. Rev. **B**, 74, 121302 (2006). DOI: 10.1103/PhysRevB.74.121302

[21] Y. Zhang, W. Xiong, W. Chen, Y. Zheng. Nanomaterials, **11**, P. 338 (2021). DOI: 10.3390/nano11020338

[22] P. Iqbal, J.A. Preece, P.M. Mendes. *Supramolecular Chemistry: From Molecules to Nanomaterials* (John Wiley & Sons, Hoboken, 2012)

[23] S. Ji, F. Zhang, P. Jin, Sol. Energy Mater Sol. Cells, **95**, 3520 (2011). DOI: 10.1016/j.solmat.2011.08.015

[24] M. Li, X. Wu, L. Li, Y. Wang, D. Li, J. Pan, S. Li, L. Sun, G. Li, J. Mater. Chem. A, **2**, 4520 (2014). DOI: 10.1039/C3TA14822J

[25] W.M. Xiong, J. Shao, Y.Q. Zhang, Y. Chen, X.Y. Zhang, W.J. Chen, Y. Zheng. Phys. Chem. Chem. Phys., **20**, 14339 (2018). DOI: 10.1039/C7CP08432C

[26] L. Petit, N. Carlie, A. Humeau, G. Boudebs, H. Jain, A.C. Miller, K. Richardson. Mater. Res. Bull., **42**, 2107 (2007). DOI: 10.1016/j.materresbull.2007.09.013

[27] S.V. Mutilin, V.Ya. Prinz, V.A. Seleznev, L.V. Yakovkina. Appl. Phys. Lett., **113**, 043101 (2018). DOI: 10.1063/1.5031075

[28] V.Ya. Prinz, S.V. Mutilin, L.V. Yakovkina, A.K. Gutakovskii, A.I. Komonov. Nanoscale, **12**, 3443 (2020). DOI: 10.1039/C9NR08712E

[29] A. Kumar, S.N. Ghosh, S. Talukder, D. Chopra. ES Mater. Manuf., **23**, 974 (2024). DOI: 10.30919/esmm974

[30] K. Appavoo, D.Y. Lei, Y. Sonnefraud, B. Wang, S.T. Pantelides, S.A. Maier, R.F. Haglund. Nano Lett., **12**, 780 (2012). DOI: 10.1021/nl203782y

[31] E.U. Donev, R. Lopez, L.C. Feldman, R.F. Haglund. Nano Lett., **9**, 702 (2009). DOI: 10.1021/nl8031839

[32] W. Zhang, X. Wu, W. Wang, K. Zhang, B. Li, Y. Chen. ACS Appl. Electron. Mater., **4**, 2101 (2022). DOI: 10.1021/acsaelm.2c00257

[33] A.I. Komonov, N.D. Mantsurov, B.V. Voloshin, V.A. Seleznev, S.V. Mutilin. Appl. Surf. Sci., **658**, 159869 (2024). DOI: 10.1016/j.apsusc.2024.159869

[34] Y.K. Ryu, R. Garcia. Nanotechnology, **28**, 142003 (2017). DOI: 10.1088/1361-6528/aa5651

[35] K.E. Kapoguzov, S.V. Mutilin, N.I. Lysenko, V.N. Kichay, L.V. Yakovkina, B.V. Voloshin, V.A. Seleznev. Physica E, **167**, 116165 (2025). DOI: 10.1016/j.physe.2024.116165

[36] A.I. Komonov, N.D. Mantsurov, B.V. Voloshin, V.A. Seleznev, S.V. Mutilin. in: Young Prof. (Ed.), IEEE 23nd Int. Conf. Electron Devices Mater IEEE, P. 20–24 (2022). DOI: 10.1109/EDM55285.2022.9855164

[37] N.D. Mantsurov, A.I. Komonov, S.V. Mutilin, V.N. Kichay, L.V. Yakovkina, Proceed. RHEAS, **1**, 48 (2024). DOI: 10.17212/1727-2769-2024-1-48-61

[38] N.D. Mantsurov, A.I. Komonov, B.V. Voloshin. *Tez. dokl. 17-i Vseross. Nauch. konf. molodykh uchenykh „Nauka. Tekhnologii. Innovatsii“* (Novosibirsk, Rossiya, 2023) (in Russian).

[39] N.D. Mantsurov, A.I. Komonov, B.V. Voloshin, V.A. Seleznev, S.V. Mutilin. in: Young Prof. (Ed.), IEEE 25nd Int. Conf. Electron Devices Mater IEEE, P. 250–254 (2024). DOI: 10.1109/EDM61683.2024.10615063

[40] K. Henkel, H. Gargouri, B. Gruska, M. Arens, M. Tallarida, D. Schmeiber. J. Vac. Sci. Technol. A, **32**, 01A107 (2014). DOI: 10.1116/1.4831897

[41] J. Haeberle, K. Henkel, H. Gargouri, F. Naumann, B. Gruska, M. Arens, M. Tallarida, D. Schmeiber. Beilstein J. Nanotechnol., **4**, 732 (2013). DOI: 10.3762/bjnano.4.83

[42] A. Mahmoodinezhad, C. Janowitz, F. Naumann, P. Plate, H. Gargouri, K. Henkel, D. Schmeiber, J.I. Flege. J. Vac. Sci. Technol. A. American Vacuum Society, **38**, 022404 (2020). DOI: 10.1116/1.5134800
[43] T. Blanquart, J. Niinisto, M. Gavagnin, V. Longo, M. Heikkila, E. Puukilainen, V.R. Pallem, C. Dussarrat, M. Ritala, M. Leskela. RSC Adv., **3**, 1179 (2013). DOI: 10.1039/C2RA22820C
[44] G. Rampelberg, M. Schaekers, K. Martens, Q. Xie, D. Deduytsche, B. Schutter, N. Blasco, J. Kittl, C. Detavernier. Appl. Phys. Lett., **98**, 162902 (2011). DOI: 10.1063/1.3579195
[45] G. Silversmit, D. Depla, H. Poelman, G.B. Marin, R. De Gryse. J. Electron Spectrosc. Relat. Phenom., **135**, 167 (2004). DOI: 10.1016/j.elspec.2004.03.004
[46] D. Necas, P. Klapetek. Cent. Eur. J. Phys., **10**, 181 (2012). DOI: 10.2478/s11534-011-0096-2
[47] P. Schilbe. Phys. B: Condens. Matter, 316–317, 600 (2002). DOI: 10.1016/S0921-4526(02)00584-7
[48] F. Urena-Begara, A. Crunteanu, J.P. Raskin. Appl. Surf. Sci., **403**, 717 (2017). DOI: 10.1016/j.apsusc.2017.01.160.
[49] K.E. Kapoguzov S.V. Mutilin V.Y. Prinz. in: Young Prof. (Ed.), IEEE 22nd Int. Conf. Electron Devices Mater IEEE, P. 58–61 (2021). DOI: 10.1109/EDM52169.2021.9507652
[50] R.G. Keil, R.E. Salomon. J. Electrochem. Soc., **112**, 643 (1965). DOI: 10.1149/1.2423631

Translated by M.Shevelev